Superposition of two-mode squeezed states for quantum information processing and quantum sensing

Fernando R. Cardoso [1,*] Daniel Z. Rossatto [2] Gabriel P. L. M. Fernandes [1]
Gerard Higgins [3] and Celso J. Villas-Boas [1]

[1]*Departamento de Física, Universidade Federal de São Carlos, 13565-905 São Carlos, São Paulo, Brazil*
[2]*Universidade Estadual Paulista (Unesp), Campus Experimental de Itapeva, 18409-010 Itapeva, São Paulo, Brazil*
[3]*Department of Physics, Stockholm University, 106 91 Stockholm, Sweden*

(Received 3 February 2021; accepted 17 May 2021; published 2 June 2021)

We investigate superpositions of two-mode squeezed states (TMSSs), which have potential applications in quantum information processing and quantum sensing. We study some properties of these nonclassical states such as the statistics of each mode and the degree of entanglement between the two modes, which can be higher than that of a TMSS with the same degree of squeezing. The states we consider can be prepared by inducing two-mode Jaynes-Cummings and anti-Jaynes-Cummings interactions in a system of two modes and a spin-$\frac{1}{2}$ particle, for instance, in the trapped ion domain, as described here. We show that when two harmonic oscillators are prepared in a superposition of two TMSSs, each reduced single-mode state can be advantageously employed to sense arbitrary displacements of the mode in phase space. The Wigner function of this reduced state exhibits a symmetrical peak centered at the phase-space origin, which has the convenient peculiarity of getting narrower in both quadratures simultaneously as the average photon number increases. This narrow peak can be used as the pointer of our quantum sensor, with its position in phase space indicating the displacement undergone by the oscillator.

DOI: 10.1103/PhysRevA.103.062405

I. INTRODUCTION

In quantum mechanics, the superposition principle is the origin of fascinating nonclassical attributes of quantum states such as quantum coherence [1], squeezing [2], and entanglement [3]. Great efforts, both theoretical and experimental, have been made in order to generate nonclassical states and to investigate their properties, since these states have a wide range of applications in quantum information processing [4–10], quantum-enhanced metrology [11–14], and fundamental tests of quantum mechanics [15,16].

Consider the two-mode squeezed state (TMSS), which is an entangled state of two bosonic modes [2]. This kind of correlation exhibits Bell nonlocality [15], a key ingredient to demonstrate the Einstein-Podolsky-Rosen paradox [17,18] (fundamental test of quantum mechanics), to implement quantum teleportation in continuous variables [19] (manipulation of quantum information), and to detect very weak fields [20] such as the gravitational waves [21] (quantum metrology). Another intriguing nonclassical state is the so-called cat state, a quantum superposition of two diametrically opposed coherent states, which has been employed to demonstrate Schrödinger's famous cat paradox and has been used as a resource for quantum information processing [22–40].

Here we are interested in nonclassical states that connect the concepts of both TMSSs and cat states, namely, a superposition of TMSSs with the same amplitudes but opposite phases. There are already theoretical proposals for their generation in microwave cavities [41] (that could also be adapted for the context of optical cavities or solid-state-based systems), in trapped ions [42], and by using the parity operator [43]. Nevertheless, the literature lacks studies of their properties and applications, which is our goal here.

We first analyze the statistics of each reduced single-mode state (RSMS) of a superposition of TMSSs. For the symmetrical balanced superposition, which we call the even TMSS, we show that there is bosonic superbunching [44,45], an effect with potential applications for advanced imaging techniques (such as ghost interference and imaging) as well as efficient nonlinear light-matter interaction [46–52]. In contrast, for small squeezing parameters, each single mode of the asymmetrical balanced superposition (odd TMSS) presents two-photon anticorrelation [44,45], a desired behavior for single-photon sources [53]. Remarkably, each mode of the even and odd TMSSs behaves as a pseudothermal state, which consists of thermal states with only even and odd Fock excitations, respectively. In addition, we investigate the entanglement degree between the modes of such catlike states, which can be higher than that of the TMSS in certain parameter regimes. Since entanglement is a resource of quantum states, this may be an advantage for quantum information processing.

Afterward, we show that the RSMS of either the even or the odd TMSS can be used to sense the amplitude of arbitrary single-mode displacements acting on a harmonic oscillator. The Wigner functions of these RSMSs each have a symmetrical peak centered at the phase-space origin, which gets

*frc@df.ufscar.br

narrower in both quadratures simultaneously as the squeezing parameter and the average number of excitations in the state increase, but without violating Heisenberg's uncertainty relation. This narrow peak works as the pointer of our quantum sensor, with its position in the phase space indicating the displacement undergone by the oscillator, which could physically describe, for instance, an optical [40] or a microwave resonator mode [35,54,55], vibrational modes of trapped ions [42,56], or a nanomechanical oscillator [57]. In this sense, our sensor is able to probe any time-dependent classical force inducing a displacement on a quantum resonator [58].

Several studies have attempted to figure out the ultimate limits of measuring forces and displacements on an oscillator [59], beating the standard quantum limit and even reaching the Heisenberg one [11,54,60–66]. However, it worth stressing that this is not our goal. Hence, as similarly considered in Ref. [58], which described the determination of both parameters of a displacement acting on an oscillator, the idea we put forward here is the possibility of sensing displacements undergone by a quantum resonator with a single-mode sensor state robust against phase errors when measuring a phase-space quadrature. Furthermore, our results hold regardless of the displacement strength, not being limited to small amplitudes as is the case for grid states [58].

The paper is organized as follows. Section II outlines the procedure for generating superpositions of TMSSs by coupling a two-level quantum system with two bosonic field modes and presents the expressions for the two-mode superposition and the reduced density matrices. In Sec. III we present the relevant statistical properties for those states, such as Wigner functions and populations in the Fock basis, and also the second-order correlation function $g^{(2)}(0)$, discussing the properties of antibunching and superbunching, and show that odd TMSSs can be used as a source of single photons in two modes. Section IV provides the entanglement properties of the superpositions of TMSSs and shows that, for a certain regime of parameters, the superpositions of TMSSs show more entanglement than TMSSs. In Sec. V we present basic concepts of quantum metrology and discuss potential applications of even and odd TMSSs in detecting small coherent forces in any direction (they are sensitive to displacements in all directions in phase space). In Sec VI a simulation of the process for generating even and odd TMSSs in the trapped-ion domain is presented. The process involves coupling the electronic state of the ion with two of its motional degrees of freedom using a two-color laser field. We also discuss the process of probing the Wigner function. Section VII summarizes the results and presents the conclusions.

II. GENERATION OF SUPERPOSITION OF TWO-MODE SQUEEZED STATES

Two-mode squeezed states can be generated by coupling two bosonic modes with a two-level quantum system (a qubit) via the Hamiltonian ($\hbar = 1$)

$$\begin{aligned}\mathcal{H} &= -(\chi^* ab + \chi a^\dagger b^\dagger)\sigma_x \\ &= -(\chi^* ab\sigma^+ + \chi a^\dagger b^\dagger \sigma^-) - (\chi^* ab\sigma^- + \chi a^\dagger b^\dagger \sigma^+),\end{aligned} \tag{1}$$

where χ is the coupling strength; a ($a^\dagger$) and b ($b^\dagger$) are the annihilation (creation) operators for the bosonic modes; $\sigma_x = |+\rangle\langle+| - |-\rangle\langle-|$ is the Pauli-X operator, with $|\pm\rangle = \frac{1}{\sqrt{2}}(|g\rangle \pm |e\rangle)$, where $|e\rangle$ ($|g\rangle$) is the excited (ground) state of the two-level system; and $\sigma^\pm = \frac{1}{2}(\sigma_x \pm i\sigma_y)$ are the fermionic raising and lowering operators. The two terms in the second line of Eq. (1) are a two-mode Jaynes-Cummings interaction and a two-mode anti-Jaynes-Cummings interaction.

The coupling Hamiltonian $\mathcal{H}$ can be realized in various platforms. In Sec. VI we describe how it may be implemented in a trapped-ion setup.

We consider the case where the two-level system is initially in the superposition state $|\phi_0\rangle = \frac{1}{\sqrt{2}}(|-\rangle + e^{i\varphi}|+\rangle) \equiv [\cos(\varphi/2)|g\rangle + i\sin(\varphi/2)|e\rangle]$ while the two bosonic modes are both in the vacuum state $|\psi_0\rangle = |0,0\rangle$. Thus the initial state of the composite system is separable $|\Psi_0\rangle = |\phi_0\rangle|\psi_0\rangle$ (the tensor product symbol is omitted for brevity). After applying the coupling $\mathcal{H}$ for time τ the composite system evolves to

$$|\Psi_\tau\rangle = e^{-i\mathcal{H}\tau}|\Psi_0\rangle = \frac{1}{\sqrt{2}}[|-\rangle|\psi(\xi)\rangle + e^{i\varphi}|+\rangle|\psi(-\xi)\rangle], \tag{2}$$

where

$$\begin{aligned}|\psi(\xi)\rangle &= e^{(\xi^* ab - \xi a^\dagger b^\dagger)}|0,0\rangle \\ &= \frac{1}{\cosh r}\sum_{n=0}^{\infty}(-e^{i\theta}\tanh r)^n |n,n\rangle\end{aligned} \tag{3}$$

is the TMSS which we parametrize by $\xi = -i\chi\tau = re^{i\theta}$, with the squeezing parameter $r = |\chi|\tau$ and squeezing angle $\theta = \arg(\xi)$ [67].

From Eq. (2) the bosonic modes are projected onto a TMSS by measurement of the two-level system in the X basis $\{|+\rangle, |-\rangle\}$. Starting from the TMSS, the reduced density matrix of one mode (found by tracing out the variables of the other mode) is a thermal state

$$\rho_{\rm th} = (1-\lambda_r)\sum_{n=0}^{\infty}\lambda_r^n |n\rangle\langle n| = \sum_{n=0}^{\infty}\frac{\langle n\rangle_{\rm th}^n}{(1+\langle n\rangle_{\rm th})^{n+1}}|n\rangle\langle n|, \tag{4}$$

with the average number of excitations $\langle n\rangle_{\rm th} = {\rm Tr}(a^\dagger a\rho_{\rm th}) = \sinh^2 r = \frac{\lambda_r}{1-\lambda_r}$ and $\lambda_r = \tanh^2 r$ [67].

More interesting results emerge when the two-level system is projected onto the Z basis $\{|e\rangle, |g\rangle\}$. In this basis Eq. (2) becomes

$$|\Psi(\xi,\varphi)\rangle = \frac{1}{2\mathcal{N}_+}|g\rangle|\psi_+(\xi,\varphi)\rangle - \frac{1}{2\mathcal{N}_-}|e\rangle|\psi_-(\xi,\varphi)\rangle, \tag{5}$$

where

$$|\psi_\pm(\xi,\varphi)\rangle = \mathcal{N}_\pm[|\psi(\xi)\rangle \pm e^{i\varphi}|\psi(-\xi)\rangle] \tag{6}$$

are superposition states of two diametrically opposed TMSSs, with $|\mathcal{N}_\pm|^2 = \frac{1}{2}\frac{1+\lambda_r}{(1+\lambda_r)\pm\epsilon_\varphi(1-\lambda_r)}$ and $\epsilon_\varphi = \cos\varphi$. When the two-level system is projected onto $|g\rangle$ ($|e\rangle$) the bosonic modes are projected onto the catlike state $|\psi_+(\xi,\varphi)\rangle$ [$|\psi_-(\xi,\varphi)\rangle$]. Since $\varphi \in [0, 2\pi)$ and $|\psi_+(\xi,\varphi)\rangle = |\psi_-(\xi,\varphi+\pi)\rangle$, it is sufficient to analyze just the properties of one of these states, e.g., $|\psi_+(\xi,\varphi)\rangle$. We refer to the states that emerge

when $\varphi = 0$ and $\varphi = \pi$ as even and odd TMSSs, respectively, $|\psi_E(\xi)\rangle \equiv |\psi_+(\xi, 0)\rangle = |\psi_-(\xi, \pi)\rangle$ and $|\psi_O(\xi)\rangle \equiv |\psi_+(\xi, \pi)\rangle = |\psi_-(\xi, 0)\rangle$, because they comprise only even and odd bosonic excitations

$$|\psi_E(\xi)\rangle = \sqrt{1-\lambda_r^2}\sum_{n=0}^{\infty}\left(-\lambda_r^{1/2}e^{i\theta}\right)^{2n}|2n, 2n\rangle, \tag{7}$$

$$|\psi_O(\xi)\rangle = \sqrt{\frac{1-\lambda_r^2}{\lambda_r}}\sum_{n=0}^{\infty}\left(-\lambda_r^{1/2}e^{i\theta}\right)^{2n+1}|2n+1, 2n+1\rangle. \tag{8}$$

When the two modes are in the state $|\psi_+(\xi, \varphi)\rangle$ the reduced density matrix of each mode is

$$\rho(r, \varphi) = 2(1-\lambda_r)|\mathcal{N}_+|^2\sum_{n=0}^{\infty}\lambda_r^n[1+(-1)^n\cos\varphi]|n\rangle\langle n|, \tag{9}$$

which is independent of the squeezing angle θ. Specifically for the even and odd TMSSs, we have the RSMSs

$$\rho_E = \left(1-\lambda_r^2\right)\sum_{n=0}^{\infty}\lambda_r^{2n}|2n\rangle\langle 2n|, \tag{10}$$

$$\rho_O = \left(1-\lambda_r^2\right)\sum_{n=0}^{\infty}\lambda_r^{2n}|2n+1\rangle\langle 2n+1|. \tag{11}$$

As the even and odd TMSSs [Eqs. (7) and (8)] are built from the superposition of TMSSs, whose reduced single-mode states are described by thermal states [Eq. (4)], it is not surprising that the reduced single modes of the even and odd TMSSs behave as pseudothermal states. We can indeed identify that by rewriting Eqs. (10) and (11) in terms of $\langle n\rangle_{\rm th}$ and comparing them with $\rho_{\rm th}$, namely,

$$\rho_E = \frac{1+2\langle n\rangle_{\rm th}}{1+\langle n\rangle_{\rm th}}\sum_{n=0}^{\infty}\frac{\langle n\rangle_{\rm th}^{2n}}{(1+\langle n\rangle_{\rm th})^{2n+1}}|2n\rangle\langle 2n|, \tag{12}$$

$$\rho_O = \frac{1+2\langle n\rangle_{\rm th}}{\langle n\rangle_{\rm th}}\sum_{n=0}^{\infty}\frac{\langle n\rangle_{\rm th}^{2n+1}}{(1+\langle n\rangle_{\rm th})^{(2n+1)+1}}|2n+1\rangle\langle 2n+1|. \tag{13}$$

From these expressions one can recognize ρ_E and ρ_O as even and odd thermal states (pseudothermal states), respectively [68], which are particular cases of binomial negative states [69]. Even thermal states (even RSMSs) can also be generated through a parametric pumping field with fluctuations [70].

III. STATISTICAL PROPERTIES

Let us discuss the properties of each single mode of the catlike state. Since $\rho(r, \varphi)$ is diagonal in the Fock basis, with populations $P_n(\varphi) = 2(1-\lambda_r)|\mathcal{N}_+|^2\lambda_r^n[1+(-1)^n\cos\varphi]$, the Wigner function of this state can be written as $W(q, p) = \sum_{n=0}^{\infty}P_nW_n(q, p)$, in which $W_n(q, p) = (2/\pi)(-1)^nL_n(4s^2)e^{-2s^2}$ is the Wigner function of the Fock state $|n\rangle$, with the Laguerre polynomial $L_n(x)$ and $s^2 = q^2 + p^2$. Here q and p are the eigenvalues of the position and momentum quadrature operators of the mode $\hat{q} = a + a^\dagger$ and $\hat{p} = i(a^\dagger - a)$, respectively, representing the dimensionless amplitudes of the mode quadratures in phase space [71].

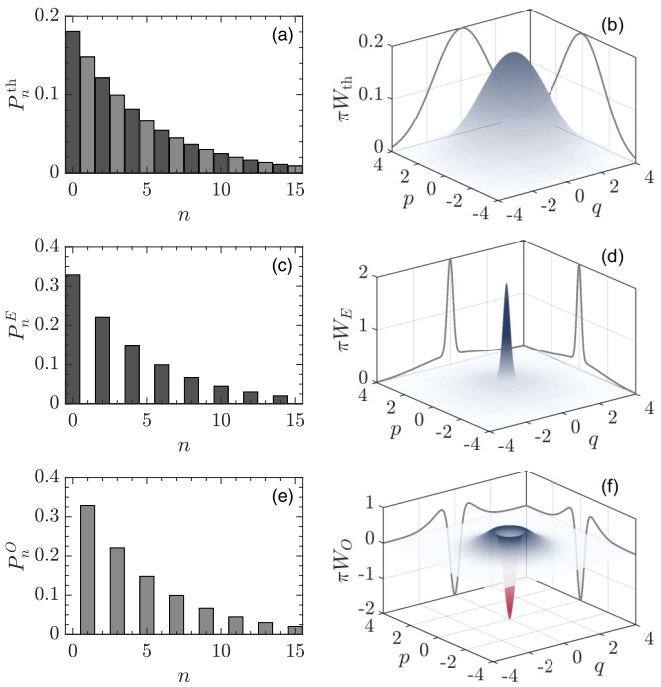

FIG. 1. Statistical properties of the reduced single-mode states: populations in the Fock basis of the (a) thermal state ($P_n^{\rm th}$) and for each mode of the (c) even (P_n^E) and (e) odd (P_n^O) TMSSs for the squeezing parameter $r = 1.5$ (light gray for odd occupation) and (b), (d), and (f) Wigner functions for the same reduced single-mode states, respectively.

First we observe that $\rho(r, \varphi)$ reduces to the thermal state $\rho_{\rm th}$ when $\varphi = \{\frac{\pi}{2}, \frac{3\pi}{2}\}$ because $|\psi_+(\xi, \varphi = \frac{\pi}{2}, \frac{3\pi}{2})\rangle$ reduces to $|\psi(\xi)\rangle$ except for a global phase factor. The Wigner function of the thermal state $\rho_{\rm th}$ is given by the two-dimensional Gaussian function

$$W_{\rm th}(q, p) = \frac{2}{\pi}\frac{\exp\left(-2\frac{(q^2+p^2)}{2\langle n\rangle_{\rm th}+1}\right)}{2\langle n\rangle_{\rm th}+1} = \frac{2}{\pi}\frac{1-\lambda_r}{1+\lambda_r}\exp\left(-2\frac{1-\lambda_r}{1+\lambda_r}(q^2+p^2)\right), \tag{14}$$

while for each single mode of the even (ρ_E) and odd (ρ_O) TMSSs the Wigner functions are each described by sums of two two-dimensional Gaussian functions

$$W_{E_O}(q, p) = \varpi_{E_O}\left((1-\lambda_r)\exp\left[-2\left(\frac{1-\lambda_r}{1+\lambda_r}\right)(q^2+p^2)\right] \pm (1+\lambda_r)\exp\left[-2\left(\frac{1+\lambda_r}{1-\lambda_r}\right)(q^2+p^2)\right]\right), \tag{15}$$

with $\varpi_E = \pi^{-1}$ and $\varpi_O = (\pi\lambda_r)^{-1}$.

Figure 1 shows the populations and the Wigner function for $\rho_{\rm th}$ ($P_n^{\rm th}$ and $W_{\rm th}$), ρ_E (P_n^E and W_E), and ρ_O (P_n^O and W_O) for the squeezing parameter $r = 1.5$. We observe that the profile of the populations for ρ_E and ρ_O are very similar, namely, $P_{2n+1}^O = P_{2n}^E = (1-\lambda_r^2)\lambda_r^{2n}$, that is, the probability distribu-

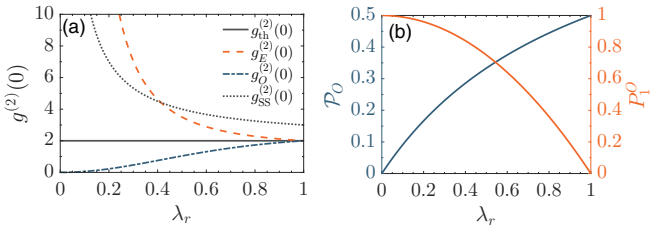

FIG. 2. (a) Second-order correlation function at zero-time delay $g^{(2)}(0)$ as a function of the squeezing parameter r, via $\lambda_r = \tanh^2(r)$, for the thermal state ($\rho_{\rm th}$) (black solid line), the RSMSs of the even (ρ_E) (orange dashed line) and odd (ρ_O) (blue dot-dashed line) TMSSs, and the single-mode squeezed state ($|{\rm SS}\rangle$) (black dotted line). (b) Probability of projecting onto the odd TMSS ($\mathcal{P}_O$) (ascending blue line) and probability of it having a single-photon in each mode (P_1^O) (descending orange line) as a function of λ_r.

tion of ρ_O is shifted by one unit compared with the distribution of ρ_E.

Accordingly, the average number of excitations is related by $\langle n\rangle_O = \langle n\rangle_E + 1$, where $\langle n\rangle_E = {\rm Tr}(a^\dagger a \rho_E) = 2\lambda_r^2/(1-\lambda_r^2)$. Moreover, we notice that P_n^E and P_n^O are very similar to $P_n^{\rm th}$, except for a normalization factor and for being nonzero only for even and odd Fock numbers, respectively, which illustrates the pseudothermal behavior of each mode of the even and odd TMSSs. It is also important to notice in Fig. 1 a concentrated profile of Wigner functions around the phase-space origin for both ρ_E and ρ_O, which can be useful for metrological purposes, as we discuss in Sec. V.

We can also investigate the statistics of ρ_E and ρ_O using the second-order correlation function at zero-time delay $g^{(2)}(0) = \langle a^\dagger a^\dagger a a\rangle/\langle a^\dagger a\rangle^2$,

$$g_E^{(2)}(0) = 2 + \frac{1-\lambda_r^2}{2\lambda_r^2} \geqslant 2 \quad \text{for } \rho_E, \tag{16}$$

$$g_O^{(2)}(0) = 2 - \frac{2\left(1-\lambda_r^2\right)}{\left(1+\lambda_r^2\right)^2} \leqslant 2 \quad \text{for } \rho_O. \tag{17}$$

For large values of the squeezing parameter ($\lambda_r \to 1$ or, equivalently, for $r \gg 1$) we observe that the correlation functions $g^{(2)}(0)$ of ρ_E and ρ_O become indistinguishable and tend to the thermal one, i.e., $g_{\rm th}^{(2)}(0) = 2$. In contrast, when the squeezing parameter is small, the RSMSs of the even and odd TMSSs present completely opposite statistics: While ρ_O exhibits antibunching [$g_O^{(2)}(0) < 1$], ρ_E displays superbunching [$g_E^{(2)}(0) > 2$]. To be more specific, $g_E^{(2)}(0) > 2\,\forall\, r \geqslant 0$ ($\lambda_r \geqslant 0$) and $g_O^{(2)}(0) < 1$ for $0 \leqslant \lambda_r < \sqrt{\sqrt{5}-2} \approx 0.49 \leftrightarrow 0 \leqslant r < \tanh^{-1}\sqrt[4]{\sqrt{5}-2} \approx 0.86$. Figure 2(a) displays the change of $g^{(2)}(0)$ with λ_r for $\rho_{\rm th}$, ρ_E, ρ_O and the single-mode squeezed state $|{\rm SS}\rangle = e^{(re^{-i\theta}a^2 - re^{i\theta}a^{\dagger 2})/2}|0\rangle$, with $g_{\rm SS}^{(2)}(0) = 2 + 1/\lambda_r$. We have included the latter for the sake of comparison, since it has the same average number of excitations of each single mode of the TMSS ($\langle n\rangle_{\rm SS} = \langle n\rangle_{\rm th}$) and presents superbunching. Remarkably, each mode of the even TMSS exhibits more superbunching than if it were in a single-mode squeezed state [$g_E^{(2)}(0) > g_{\rm SS}^{(2)}(0) > 2$] within the parameter range $0 \leqslant \lambda_r < \sqrt{2}-1 \approx 0.41 \leftrightarrow 0 \leqslant r < \tanh^{-1}\sqrt{\sqrt{2}-1} \approx 0.76$.

Due to the aforementioned attributes, each mode of the even and odd TMSSs is quite suitable for quantum devices related to advanced imaging techniques and single-photon generation, respectively. A single photon may be produced in each of the two modes when the odd TMSS is produced. The probability of projecting onto the odd TMSS is $\mathcal{P}_O = \lambda_r/(1+\lambda_r)$. The proportion of the odd TMSS described by two single photons is $P_1^O = 1-\lambda_r^2$. Production of high-purity states of two single photons requires $\lambda_r \to 0$, which comes at the expense of a low production probability $\mathcal{P}_O$, as shown in Fig. 2(b). It is worth noting that the qubit may be used to herald projection onto the odd TMSS.

IV. ENTANGLEMENT

Considering a bipartite system in a pure state, the degree of entanglement between the subsystems can be quantified through the linear entropy $E = \frac{d}{d-1}(1-\gamma)$, where $\gamma = {\rm Tr}(\rho_1^2)$ is the purity of one of the subsystems described by the reduced density matrix ρ_1 and $d = \dim \rho_1$. Since our subsystems are bosonic modes, with infinite-dimensional Hilbert spaces, $0 \leqslant E \leqslant 1$ such that $E = 0$ for separable states while $E = 1$ for maximally entangled continuous-variable states.

For the TMSS $|\psi(\xi)\rangle$, the degree of entanglement is

$$E_{\rm TMSS}(r) = 1 - \frac{1-\lambda_r}{1+\lambda_r}, \tag{18}$$

while for the general superposition $|\psi_+(\xi,\varphi)\rangle$,

$$E_\varphi(r) = 1 - \left(\frac{1-\lambda_r^2}{1+\lambda_r^2}\right)\frac{(1+\epsilon_\varphi)^2 + \lambda_r^2(1-\epsilon_\varphi)^2}{[(1+\epsilon_\varphi) + \lambda_r(1-\epsilon_\varphi)]^2}. \tag{19}$$

Here $E_\varphi(r) = E_{\rm TMSS}(r)$ for any r when $\varphi = \{\frac{\pi}{2}, \frac{3\pi}{2}\} \to \epsilon_\varphi = 0$, which is not a surprise, since we have seen in Sec. III that $\rho(r,\varphi)$ reduces to $\rho_{\rm th}$ for these values of φ. The same degree of entanglement also occurs when $\lambda_r = \sqrt{(1+\epsilon_\varphi)/(1-\epsilon_\varphi)}$ or $r \to \infty$. Notably, $E_\varphi(r) > E_{\rm TMSS}(r)$ for $\varphi \in (\frac{\pi}{2}, \pi) \cup (\pi, \frac{3\pi}{2})$ provided $0 < \lambda_r < \sqrt{(1+\epsilon_\varphi)/(1-\epsilon_\varphi)}$. In this range, for the same value of the squeezing parameter r, the entanglement degree in the catlike TMSSs becomes higher than that in the TMSS. Curiously, it can reach high values even for $r \ll 1$, namely, $E_\varphi(r) \approx 0.5$ for $\varphi = \pi + \beta$ and $r \approx |\beta|/2$ considering $|\beta| \ll 1$, for which we have $|\psi_+(\xi,\varphi)\rangle \approx (|0,0\rangle - {\rm sgn}(\beta)e^{i(\theta+\pi/2)}|1,1\rangle)/\sqrt{2}$, i.e., a maximally entangled qubit state. By contrast, $E_{\rm TMSS}(r) \approx \beta^2/2 \ll 1$ under the same conditions, for which we have $|\psi(\xi)\rangle \approx (|0,0\rangle - (|\beta|/2)e^{i\theta}|1,1\rangle)/\sqrt{1+|\beta|^2/4} \approx |0,0\rangle$, i.e., a separable state. This means that it is possible to generate much more entanglement between the modes with a lower squeezing parameter by exploiting the catlike states instead of the TMSS, indicating an advantage from the point of view of quantum information science. Figure 3 illustrates the above results. It is worth noting that the even ($\varphi = 0$) and odd ($\varphi = \pi$) TMSSs have the same entanglement degree $E_E(r) = E_O(r) = 1 - (1-\lambda_r^2)/(1+\lambda_r^2)$, which is always smaller than or equal to that for the TMSS. Despite that, we show in the next section that their RSMSs can be employed for quantum metrological purposes.

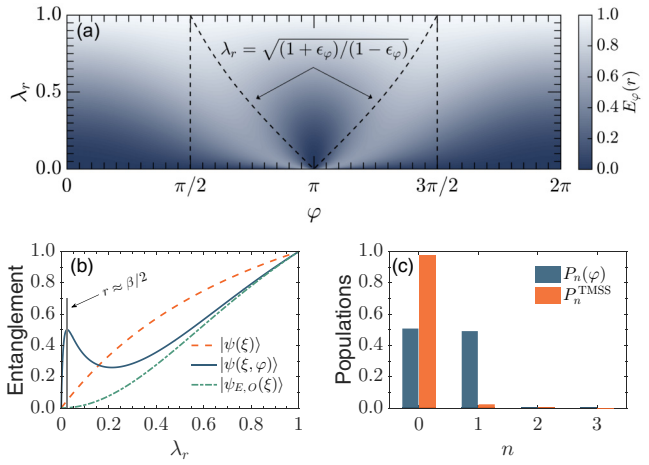

FIG. 3. (a) Density plot showing the entanglement between the two modes $[E_\varphi(r)]$, when they are in the catlike state $|\psi_+(r,\varphi)\rangle$, as a function of the initial-state relative phase φ and the two-mode squeezing parameter r via $\lambda_r = \tanh^2(r)$. The dashed lines delimit the region for which $E_\varphi(r)$ surpasses the entanglement of the TMSS $[E_{\mathrm{TMSS}}(r)]$. (b) Entanglement degree as a function of λ_r corresponding to the states $|\psi(\xi)\rangle$ (orange dashed line), $|\psi(\xi,\varphi)\rangle$ (blue solid line), and $|\psi_{E,O}(\xi)\rangle$ (green dot-dashed line), considering $\varphi = \pi + \beta$, with $\beta = \pi/10$. One can notice here that the entanglement outperforming occurs even for small values of r, reaching its maximum for $r \approx |\beta|/2$ ($\lambda_r \approx r^2$) when $|\beta| \ll 1$. Surprisingly, under this condition an extreme contrast between the entanglement in the catlike state and in the TMSS takes place; while the latter is essentially a separable state given by the two-mode ground state $[|\psi(\xi)\rangle \approx (|0,0\rangle - (|\beta|/2)e^{i\theta}|1,1\rangle)/\sqrt{1+|\beta|^2/4} \to E_{\mathrm{TMSS}}(r) \approx 0.05$ for the considered parameters], the former is approximately a maximally entangled qubit state $[|\psi_+(\xi,\varphi)\rangle \approx (|0,0\rangle - ie^{i\theta}|1,1\rangle)/\sqrt{2} \to E_\varphi(r) \approx 0.5]$. The even and odd TMSSs have the same entanglement degree, which is always smaller than or equal to that for the TMSS. (c) Populations of the catlike state $[P_n(\varphi)]$ [blue (dark gray) bars] and the TMSS (P_n^{TMSS}) [orange (light gray) bars] for $r = \beta/2$ and $\varphi = \pi + \beta$, with $\beta = \pi/10$.

V. QUANTUM METROLOGY

Quantum metrology takes advantage of the properties of quantum mechanics to better estimate parameters involved in dynamical processes, using quantum states as probes [72]. The process of estimating a parameter y follows a specific sequence of steps, known as the protocol of estimation [73]: (i) The probe state is prepared in an initial and determined configuration, represented by the density matrix ρ; (ii) the initial state evolves through a dynamical process, which is represented by a unitary evolution operator $U(y)$ such that the final configuration of the system is dependent on the parameter y; (iii) the final state $\rho(y)$ is measured, giving results $y_{\mathrm{est}}(\kappa)$, with associated probabilities $P_\kappa(y)$; (iv) these results are used to estimate the parameter y. It is important to note that different results κ come from separate processes of measurement. The average value of the parameter can then be calculated with the individual estimation $y_{\mathrm{est}}(\kappa)$ as $\langle y_{\mathrm{est}}\rangle = \sum_\kappa y_{\mathrm{est}}(\kappa)P_\kappa(y)$, with $\sum_\kappa P_\kappa(y) = 1$. The deviation of the parameter can be defined as $(\Delta y)^2 \equiv \langle (y_{\mathrm{est}} - \langle y_{\mathrm{est}}\rangle)^2\rangle$ and its lower bound is proportional to the inverse of the Fisher information $\langle (\frac{d\ln[P_\kappa(y)]}{dy})^2\rangle$ [74,75] with respect to the parameter y and represents the maximum quantity of information that can be obtained with respect to y through the probability set $\{P_\kappa(y)\}$, as derived from the Cramér-Rao inequality [76,77]. Although this is the main method of estimation of the parameter we discuss, nonlinear methods of estimation for quantum metrological purposes are also available [78–80].

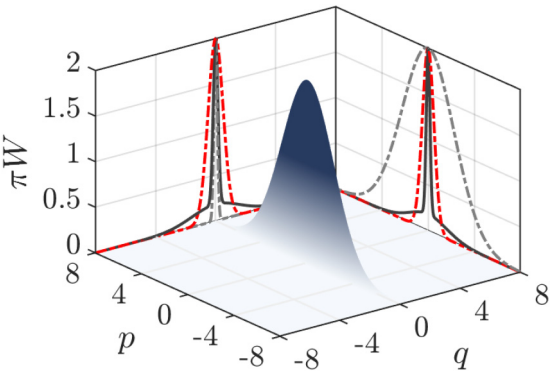

FIG. 4. Comparison of the Wigner function and its projections of the single-mode squeezed state (projections in light gray dot-dashed curves) with the projections of the RSMS of the even TMSS (black solid lines), with $r = 1.5$ and the vacuum state $|0\rangle$ (red dashed lines). The projections of the RSMS of the even TMSS display tails because they are described by the summation of two two-dimensional Gaussian functions [see Eq. (15)].

Given a generator $U(y)$ for the transformation on the density matrix which leads to the final state $\rho(y)$, the quantum Fisher information for y with probe state ρ can be written as $F(y) = 4[\Delta U(y)]^2$ if ρ is a pure state, with $[\Delta U(y)]^2 = \langle U^2(y)\rangle - \langle U(y)\rangle^2$, and $F(y) = 2\sum_{i,j}\frac{(\delta_i-\delta_j)^2}{\delta_i+\delta_j}|\langle i|U(y)|j\rangle|^2$ if ρ is mixed, where δ_j and $|j\rangle$ stand for the eigenvalues and eigenvectors of ρ, respectively.

Single-mode squeezed states are widely used in quantum metrology due to the reduction of fluctuations in one of the quadratures of the bosonic mode [81–83]. The fact that the Wigner functions of each mode of the even and odd TMSSs are invariant under rotations and sharply concentrated around the origin of the phase space (Fig. 1) motivates the study of applications of those states in quantum metrology.

Figure 4 shows a comparison between the Wigner functions of a single-mode squeezed state, with reduced noise in one of the quadratures, the RSMS of the even TMSS, for the same value of the squeezing parameter r, and a vacuum coherent state. The single-mode squeezed state has a more concentrated probability distribution profile than the RSMS. However, we would like to point out that the symmetry of the Wigner function (around the origin of the phase space) of the even and odd RSMSs implies a robust and sensitive scheme for applications in quantum metrology, since that peak, whose width can be controlled by the squeezing parameter r, allows for probing small displacements in any direction, as described in detail in the next section. Furthermore, the Wigner function still presents thermal contributions along broad regions of the phase space, so, despite the concentrated peak around the origin, the Heisenberg uncertainty principle

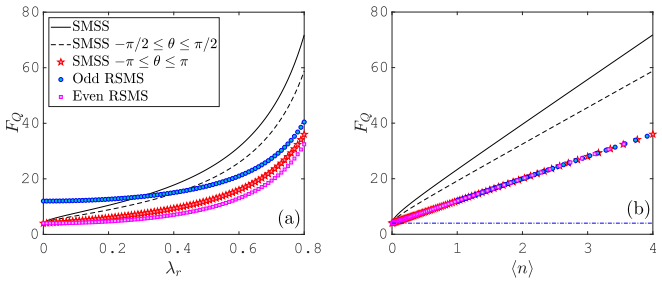

FIG. 5. (a) Quantum Fisher information F_Q as a function of λ_r and (b) average number of excitations in the bosonic field $\langle n \rangle$ for each state. If the direction of squeezing in phase space matches the displacement direction, single-mode squeezed states are well suited for measuring the displacement. This is shown by the quantum Fisher information F_Q of the solid black curve. If the angle θ between the squeezing direction and the displacement direction is large, it can be more efficient to measure the displacement using the RSMS of the even or odd TMSS. This is seen by comparing the red star curve (the black dashed and red star curves show the average F_Q values obtained with SMSSs when θ is spread over a range) with the blue circle and pink square curves. Here $\lambda_r = \tanh^2 r$ describes the amount of squeezing. Note also that for small values ($\lambda_r < 0.3$) the odd RSMS presents a larger F_Q than the SMSS. In particular, for $\lambda \to 0$, the odd RSMS (blue circles) approximates to the single-photon state $|1\rangle$ and the SMSS to the vacuum $|0\rangle$. From (b) it can be seen that F_Q behaves linearly for all states and, in particular, for small values of λ, $F_Q(\langle n \rangle) \approx 4(2\langle n \rangle + 1)$, with $\langle n \rangle$ the average number of excitations for each corresponding state. Note also that the red star, blue circle, and pink square curves overlap in (b), corresponding to the SMSS ($-\pi \leqslant \theta \leqslant \pi$) and odd and even RSMSs, respectively. We also included in (b) the quantum Fisher information for a coherent state $|\alpha\rangle$ represented by the blue dot-dashed line, which presents a constant value of $F_Q = 4.0$.

is not violated. For estimation of displacement, we employ the general quadrature operator $X(\phi) = ae^{-i\phi} + a^\dagger e^{i\phi}$, which corresponds to position and momentum operators for $\phi = 0, \pi/2$, respectively. Figure 5 shows the quantum Fisher information for the RSMSs of the even and odd TMSSs and for the single-mode squeezed state, for estimation of position amplitudes of the mode. Although the single-mode squeezed state shows better results for the quantum Fisher information (for a specific quadrature), by employing a measurement scheme of the Wigner function [84], the even and odd RSMSs could be employed to detect small coherent forces.

For our state, differently from the single-mode squeezed state, one does not need to worry about the phase of the displacement due to the symmetry of its Wigner function around the origin, as we see in Fig. 4. Thus, although both variances of the quadratures X and P increase with the amount of squeezing λ as $(3\lambda^2 + 1)/(1 - \lambda^2)$ and $(\lambda^2 + 3)/(1 - \lambda^2)$ for the even and odd RSMSs, respectively, the RSMSs still can be very useful to detect small displacements and, consequently, small forces, by monitoring the Wigner function of the reduced mode state. This is described in detail in the next section, showing in particular how these ideas can be implemented in trapped-ion systems.

VI. ION IMPLEMENTATION

Two-mode squeezed states can be generated by a combination of Jaynes-Cummings and anti-Jaynes-Cummings interactions, as we see in Eq. (1). In this section we describe how these interactions can be realized to produce an entangled state of two motional modes of a single trapped ion, which could be used for enhanced force sensing. In Ref. [42] similar effective Hamiltonians are proposed, but the proposal involves two trapped ions and other types of two-mode squeezed states are considered.

Electronic states of a single trapped ion can be coupled to the ion's motion using a laser field. When the laser field's wave vector projects onto two motional modes (x and y), the Hamiltonian describing the coupling (within the interaction picture and after taking the rotating-wave approximation) is

$$H_F = \frac{\Omega}{2} e^{-i\Delta t} e^{i\eta_x (a e^{-i\omega_x t} + a^\dagger e^{i\omega_x t})} e^{i\eta_y (b e^{-i\omega_y t} + b^\dagger e^{i\omega_y t})} \sigma^+ + \text{H.c.}, \tag{20}$$

where Ω is the coupling strength, Δ is the detuning of the laser field from the atomic resonance, $a^\dagger$, $b^\dagger$ and a, b raise and lower the states of the x and y modes, and ω_i are the motion mode frequencies. In addition, σ^+ and σ^- act on the ion's internal state and the Lamb-Dicke parameters are defined by

$$\eta_i = k_i \sqrt{\frac{\hbar}{2m\omega_i}}, \tag{21}$$

where k_i is the projection of the laser field's wave vector in the i direction and m is the ion mass.

When a two-color coupling field satisfying $\Delta = \pm(\omega_x + \omega_y)$ is used, provided the system is within the Lamb-Dicke regime $\eta_x^2(2n_x + 1)$ and $\eta_y^2(2n_y + 1) \ll 1$ (n_i is the number of phonons in the i mode), the coupling Hamiltonian becomes

$$\begin{aligned} H_{\text{eff}} &= -\tfrac{1}{2}\eta_x \eta_y \Omega \sigma^+ (ab + a^\dagger b^\dagger) + \text{H.c.} \\ &= -\tfrac{1}{2}\eta_x \eta_y \Omega \sigma_x (ab + a^\dagger b^\dagger) \end{aligned} \tag{22}$$

after another application of the rotating-wave approximation. Identifying $\chi = \frac{1}{2}\eta_x \eta_y \Omega$, this Hamiltonian is equivalent to Eq. (1) for real-valued χ.

The coupling laser field drives second-order sideband transitions which are relatively weak. This implementation requires the coupling dynamics to be faster than the decoherence time $\eta_x \eta_y \Omega \gg \gamma$, also off-resonant excitation of stronger transitions must be avoided $\Omega \ll \omega_x + \omega_y$.

If the system is initialized in $|\Psi(t = 0)\rangle = |g\rangle|0, 0\rangle$, then after evolution under H_F given by Eq. (22), followed by projection of the electronic state onto $|g\rangle$ ($|e\rangle$), the motional modes of the trapped ion can be prepared in the even (odd) TMSS in principle. Projective measurement of a trapped ion's electronic state is commonly accomplished with near-unity fidelity by detecting laser-induced fluorescence detection [56]. We note that if the ion is in state $|g\rangle$, the scattering of fluorescence photons destroys the ion's motional state. If the ion is in projected onto the nonfluorescing state ($|e\rangle$), the motional state (the odd TMSS) will be unperturbed.

In Fig. 6 we plot the fidelity of the states which evolve under the effective Hamiltonian H_{eff} [Eq. (22)] as compared with the states evolved under the full Hamiltonian H_F [Eq. (20)]. The effective Hamiltonian describes the squeezing dynam-

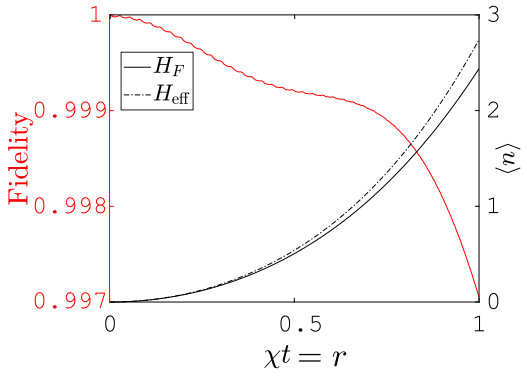

FIG. 6. The squeezing dynamics in a trapped ion system is captured well by $H_{\rm eff}$: The fidelity (represented by the red solid decreasing curve) shows the overlap of the state evolved according to the effective Hamiltonian $H_{\rm eff}$ (black dot-dashed curve) with the state evolved according to the full Hamiltonian H_F (black solid line). The evolution of the average number of excitations in the bosonic fields is also shown.

ics well up to $\chi t = r = 1$. The parameters considered are $\omega_x = 1.0$, $\omega_y = 1.2$, $\Omega = \omega_x/20$, and $\eta_x = \eta_y = 0.1$. We also show the evolution of the average number of phonons $\langle n \rangle = a^\dagger a + b^\dagger b$.

Now we describe how these states can be employed to detect small forces by measuring the Wigner function of one of the modes based on the protocol given in Ref. [84]. By tracing out one of the modes, one can see that the Wigner function of the reduced state is completely symmetric around the origin (see Fig. 4). Thus, one does not need to worry about the phase of the coherent displacement applied to the ion trap.

A weak coherent force applied on either the ion or the ion trap causes a displacement $D(\alpha) = e^{\alpha a^\dagger - \alpha^* a}$ of the mode state, resulting in a state $\rho(\alpha) = D(\alpha)\rho_v D^{-1}(\alpha)$, where ρ_v is the reduced density operator of the motional state. The phase and amplitude of the complex parameter α indicate the direction and intensity of the displacement operation in the phase space. At this point a laser pulse resonant to the $|g\rangle \leftrightarrow |e\rangle$ transition (the carrier transition) is applied, whose Hamiltonian is given by (keeping terms up to η_x^2) $H_c = \Omega/2[1 - \eta_x^2(a^\dagger a + \frac{1}{2})]\sigma_x$. Adjusting the interaction time τ such that $\Omega\eta_x^2\tau/2 = \pi/2$, the evolution operator will be given by $U = e^{-iH_c\tau} = e^{-i(\Phi - \pi a^\dagger a/2)}$, with $\Phi = \Omega\tau/2 - \pi/4$. As shown in [84], the evolved state of the system, $U\rho(\alpha)|e\rangle\langle e|U^{-1}$, will be

$$[|e\rangle \cos(\Phi - \pi a^\dagger a/2) - i|g\rangle \sin(\Phi - \pi a^\dagger a/2)]\rho(\alpha) \times [\langle e| \cos(\Phi - \pi a^\dagger a/2) + i\langle g| \sin(\Phi - \pi a^\dagger a/2)] \quad (23)$$

and then the population inversion $P_{eg} = \langle \sigma_z \rangle$ of the ion will give, apart from a constant factor, the value of the Wigner function at the position $\alpha = (q - ip)/2$ in phase space, i.e., $P_{eg} \propto W(\alpha)$ [84]. For the even (odd) TMSS, when there is no force acting on the ion, this results in $\alpha = 0$ and consequently the maximal (minimal) value of the atomic population inversion. However, for small values of $|\alpha|$, which are larger than the width of the central peak of the Wigner function, the population inversion would result in nearly zero, thus allowing us to detect the action of small coherent forces applied in any direction.

VII. CONCLUSION

In this work we have presented the statistical properties of superpositions of two-mode squeezed states with relative phase factors, giving special attention to two cases of relative phase, corresponding to the even and odd TMSSs. The reduced single-mode states of the even (ρ_E) and odd (ρ_O) TMSSs, obtained by tracing out one of the bosonic modes, present populations in the Fock basis which resemble thermal distribution, thus illustrating the pseudothermal behavior of those states. Furthermore, we investigated the second-order correlation function of ρ_E and ρ_O and showed that, for small squeezing parameters, ρ_E presents superbunching behavior, while ρ_O presents antibunching, thus making it a potential source of single photons. We studied entanglement between the two bosonic modes corresponding to the superposition of TMSSs; for small values of the squeezing parameter r and specific relative phase angle φ, the superpositions show a larger degree of entanglement than TMSSs, generating a maximally mixed state in each of the RSMSs when tracing out one of the mode variables. We also studied the pseudoprobability distributions related to ρ_E and ρ_O in phase space, given by the Wigner function $W(q, p)$. We pointed out that the profiles of both RSMSs narrow around the phase-space origin as the squeezing parameter is increased. For ρ_E and ρ_O, the symmetry of $W(q, p)$ makes the states sensible to weak forces in any direction of the phase space, in contrast with the single-mode squeezed state. Finally, we described how the states discussed above can be generated and how they can be employed to measure weak forces in the trapped-ion domain, by deriving effective two-mode Jaynes-Cummings-like interactions, thus motivating applications in quantum information processing, quantum metrology, and quantum sensing of small coherent displacements.

ACKNOWLEDGMENTS

This work was supported by the Coordenação de Aperfeiçoamento de Pessoal de Nível Superior (CAPES), Finance Code 001, and through the CAPES/STINT project, Grant No. 88881.304807/2018-01. C.J.V.-B. is grateful for support from São Paulo Research Foundation Grant No. 2019/11999-5 and the National Council for Scientific and Technological Development Grant No. 307077/2018-7. This work is also part of the Brazilian National Institute of Science and Technology for Quantum Information Grant No. 465469/2014-0. G.H. gratefully acknowledges the hospitality of Universidade Federal de São Carlos and Universidade de São Paulo.

[1] A. Streltsov, G. Adesso, and M. B. Plenio, Quantum coherence as a resource, Rev. Mod. Phys. **89**, 041003 (2017).

[2] A. I. Lvovsky, in *Fundamentals of Photonics and Physics*, edited by D. L. Andrew (Wiley, Hoboken, 2015), Vol. 1, Chap. 5, pp. 121–164.

[3] R. Horodecki, P. Horodecki, M. Horodecki, and K. Horodecki, Quantum entanglement, Rev. Mod. Phys. **81**, 865 (2009).

[4] M. A. Nielsen and I. L. Chuang, *Quantum Computation and Quantum Information* (Cambridge University, Cambridge, 2000).

[5] T. D. Ladd, F. Jelezko, R. Laflamme, Y. Nakamura, C. Monroe, and J. L. O'Brien, Quantum computers, Nature (London) **464**, 45 (2010).

[6] B. M. Terhal, Quantum error correction for quantum memories, Rev. Mod. Phys. **87**, 307 (2015).

[7] N. Gisin and R. Thew, Quantum communication, Nat. Photon. **1**, 165 (2007).

[8] V. Scarani, H. Bechmann-Pasquinucci, N. J. Cerf, M. Dušek, N. Lütkenhaus, and M. Peev, The security of practical quantum key distribution, Rev. Mod. Phys. **81**, 1301 (2009).

[9] H. J. Kimble, The quantum internet, Nature (London) **453**, 1023 (2008).

[10] R. Van Meter, *Quantum Networking (Networks and Telecommunications)* (Wiley, Hoboken, 2014).

[11] V. Giovannetti, S. Lloyd, and L. Maccone, Quantum-enhanced measurements: Beating the standard quantum limit, Science **306**, 1330 (2004).

[12] V. Giovannetti, S. Lloyd, and L. Maccone, Advances in quantum metrology, Nat. Photon. **5**, 222 (2011).

[13] G. Tóth and I. Apellaniz, Quantum metrology from a quantum information science perspective, J. Phys. A: Math. Theor. **47**, 424006 (2014).

[14] L. Pezzè, A. Smerzi, M. K. Oberthaler, R. Schmied, and P. Treutlein, Quantum metrology with nonclassical states of atomic ensembles, Rev. Mod. Phys. **90**, 035005 (2018).

[15] N. Brunner, D. Cavalcanti, S. Pironio, V. Scarani, and S. Wehner, Bell nonlocality, Rev. Mod. Phys. **86**, 419 (2014).

[16] D. Z. Rossatto, T. Werlang, E. I. Duzzioni, and C. J. Villas-Boas, Nonclassical Behavior of an Intense Cavity Field Revealed by Quantum Discord, Phys. Rev. Lett. **107**, 153601 (2011).

[17] A. Einstein, B. Podolsky, and N. Rosen, Can Quantum-Mechanical Description of Physical Reality Be Considered Complete? Phys. Rev. **47**, 777 (1935).

[18] M. D. Reid, P. D. Drummond, W. P. Bowen, E. G. Cavalcanti, P. K. Lam, H. A. Bachor, U. L. Andersen, and G. Leuchs, Colloquium: The Einstein-Podolsky-Rosen paradox: From concepts to applications, Rev. Mod. Phys. **81**, 1727 (2009).

[19] S. Pirandola, J. Eisert, C. Weedbrook, A. Furusawa, and S. L. Braunstein, Advances in quantum teleportation, Nat. Photon. **9**, 641 (2015).

[20] P. M. Anisimov, G. M. Raterman, A. Chiruvelli, W. N. Plick, S. D. Huver, H. Lee, and J. P. Dowling, Quantum Metrology with Two-Mode Squeezed Vacuum: Parity Detection Beats the Heisenberg Limit, Phys. Rev. Lett. **104**, 103602 (2010).

[21] R. Schnabel, Squeezed states of light and their applications in laser interferometers, Phys. Rep. **684**, 1 (2017).

[22] W. Schleich, M. Pernigo, and F. L. Kien, Nonclassical state from two pseudoclassical states, Phys. Rev. A **44**, 2172 (1991).

[23] B. C. Sanders, Entangled coherent states, Phys. Rev. A **45**, 6811 (1992).

[24] S. J. van Enk and O. Hirota, Entangled coherent states: Teleportation and decoherence, Phys. Rev. A **64**, 022313 (2001).

[25] H. Jeong, M. S. Kim, and J. Lee, Quantum-information processing for a coherent superposition state via a mixed entangled coherent channel, Phys. Rev. A **64**, 052308 (2001).

[26] J. Wenger, M. Hafezi, F. Grosshans, R. Tualle-Brouri, and P. Grangier, Maximal violation of Bell inequalities using continuous-variable measurements, Phys. Rev. A **67**, 012105 (2003).

[27] H. Jeong, W. Son, M. S. Kim, D. Ahn, and Č. Brukner, Quantum nonlocality test for continuous-variable states with dichotomic observables, Phys. Rev. A **67**, 012106 (2003).

[28] T. C. Ralph, A. Gilchrist, G. J. Milburn, W. J. Munro, and S. Glancy, Quantum computation with optical coherent states, Phys. Rev. A **68**, 042319 (2003).

[29] A. Gilchrist, K. Nemoto, W. J. Munro, T. C. Ralph, S. Glancy, S. L. Braunstein, and G. J. Milburn, Schrödinger cats and their power for quantum information processing, J. Opt. B **6**, S828 (2004).

[30] M. Stobińska, H. Jeong, and T. C. Ralph, Violation of Bell's inequality using classical measurements and nonlinear local operations, Phys. Rev. A **75**, 052105 (2007).

[31] A. P. Lund, T. C. Ralph, and H. L. Haselgrove, Fault-Tolerant Linear Optical Quantum Computing with Small-Amplitude Coherent States, Phys. Rev. Lett. **100**, 030503 (2008).

[32] Z. Leghtas, G. Kirchmair, B. Vlastakis, R. J. Schoelkopf, M. H. Devoret, and M. Mirrahimi, Hardware-Efficient Autonomous Quantum Memory Protection, Phys. Rev. Lett. **111**, 120501 (2013).

[33] D. J. Wineland, Nobel lecture: Superposition, entanglement, and raising Schrödinger's cat, Rev. Mod. Phys. **85**, 1103 (2013).

[34] S. Haroche, Nobel lecture: Controlling photons in a box and exploring the quantum to classical boundary, Rev. Mod. Phys. **85**, 1083 (2013).

[35] B. Vlastakis, G. Kirchmair, Z. Leghtas, S. E. Nigg, L. Frunzio, S. M. Girvin, M. Mirrahimi, M. H. Devoret, and R. J. Schoelkopf, Deterministically encoding quantum information using 100-photon Schrödinger cat states, Science **342**, 607 (2013).

[36] M. Mirrahimi, Z. Leghtas, V. V. Albert, S. Touzard, R. J. Schoelkopf, L. Jiang, and M. H. Devoret, Dynamically protected cat-qubits: A new paradigm for universal quantum computation, New J. Phys. **16**, 045014 (2014).

[37] C. Wang, Y. Y. Gao, P. Reinhold, R. W. Heeres, N. Ofek, K. Chou, C. Axline, M. Reagor, J. Blumoff, K. M. Sliwa, L. Frunzio, S. M. Girvin, L. Jiang, M. Mirrahimi, M. H. Devoret, and R. J. Schoelkopf, A Schrödinger cat living in two boxes, Science **352**, 1087 (2016).

[38] N. Ofek, A. Petrenko, R. Heeres, P. Reinhold, Z. Leghtas, B. Vlastakis, Y. Liu, L. Frunzio, S. M. Girvin, L. Jiang, M. Mirrahimi, M. H. Devoret, and R. J. Schoelkopf, Extending the lifetime of a quantum bit with error correction in superconducting circuits, Nature (London) **536**, 441 (2016).

[39] V. V. Albert, K. Noh, K. Duivenvoorden, D. J. Young, R. T. Brierley, P. Reinhold, C. Vuillot, L. Li, C. Shen, S. M. Girvin, B. M. Terhal, and L. Jiang, Performance and structure of single-mode bosonic codes, Phys. Rev. A **97**, 032346 (2018).

[40] B. Hacker, S. Welte, S. Daiss, A. Shaukat, S. Ritter, L. Li, and G. Rempe, Deterministic creation of entangled atom–light Schrödinger-cat states, Nat. Photon. **13**, 110 (2019).

[41] C. J. Villas-Bôas and M. H. Moussa, One-step generation of high-quality squeezed and EPR states in cavity QED, Eur. Phys. J. D **32**, 147 (2004).
[42] H.-S. Zeng, L.-M. Kuang, and K.-L. Gao, Two-mode squeezed states and their superposition in the motion of two trapped ions, Phys. Lett. A **300**, 427 (2002).
[43] A. Karimi, Superposition and entanglement of two-mode squeezed vacuum states, Int. J. Quantum Inf. **16**, 1850003 (2018).
[44] Z. Ficek and S. Swain, *Quantum Interference and Coherence: Theory and Experiments* (Springer, Heidelberg, 2005).
[45] H. Paul, Photon antibunching, Rev. Mod. Phys. **54**, 1061 (1982).
[46] D. Bhatti, J. von Zanthier, and G. S. Agarwal, Superbunching and nonclassicality as new hallmarks of superradiance, Sci. Rep. **5**, 17335 (2015).
[47] B. Bai, J. Liu, Y. Zhou, H. Zheng, H. Chen, S. Zhang, Y. He, F. Li, and Z. Xu, Photon superbunching of classical light in the Hanbury Brown–Twiss interferometer, J. Opt. Soc. Am. B **34**, 2081 (2017).
[48] Y. Zhou, F.-l. Li, B. Bai, H. Chen, J. Liu, Z. Xu, and H. Zheng, Superbunching pseudothermal light, Phys. Rev. A **95**, 053809 (2017).
[49] T. Lettau, H. A. M. Leymann, B. Melcher, and J. Wiersig, Superthermal photon bunching in terms of simple probability distributions, Phys. Rev. A **97**, 053835 (2018).
[50] J. Liu, J. Wang, H. Chen, H. Zheng, Y. Liu, Y. Zhou, F. li Li, and Z. Xu, High visibility temporal ghost imaging with classical light, Opt. Commun. **410**, 824 (2018).
[51] M. Marconi, J. Javaloyes, P. Hamel, F. Raineri, A. Levenson, and A. M. Yacomotti, Far-From-Equilibrium route to Superthermal Light in Bimodal Nanolasers, Phys. Rev. X **8**, 011013 (2018).
[52] L. Zhang, Y. Lu, D. Zhou, H. Zhang, L. Li, and G. Zhang, Superbunching effect of classical light with a digitally designed spatially phase-correlated wave front, Phys. Rev. A **99**, 063827 (2019).
[53] B. Lounis and M. Orrit, Single-photon sources, Rep. Prog. Phys. **68**, 1129 (2005).
[54] M. Penasa, S. Gerlich, T. Rybarczyk, V. Métillon, M. Brune, J. M. Raimond, S. Haroche, L. Davidovich, and I. Dotsenko, Measurement of a microwave field amplitude beyond the standard quantum limit, Phys. Rev. A **94**, 022313 (2016).
[55] A. Fedorov, A. K. Feofanov, P. Macha, P. Forn-Díaz, C. J. P. M. Harmans, and J. E. Mooij, Strong Coupling of a Quantum Oscillator to a Flux Qubit at Its Symmetry Point, Phys. Rev. Lett. **105**, 060503 (2010).
[56] D. Leibfried, R. Blatt, C. Monroe, and D. Wineland, Quantum dynamics of single trapped ions, Rev. Mod. Phys. **75**, 281 (2003).
[57] C. A. Regal, J. D. Teufel, and K. W. Lehnert, Measuring nanomechanical motion with a microwave cavity interferometer, Nat. Phys. **4**, 555 (2008).
[58] K. Duivenvoorden, B. M. Terhal, and D. Weigand, Single-mode displacement sensor, Phys. Rev. A **95**, 012305 (2017).
[59] C. M. Caves, K. S. Thorne, R. W. P. Drever, V. D. Sandberg, and M. Zimmermann, On the measurement of a weak classical force coupled to a quantum-mechanical oscillator. I. Issues of principle, Rev. Mod. Phys. **52**, 341 (1980).
[60] A. Facon, E.-K. Dietsche, D. Grosso, S. Haroche, J.-M. Raimond, M. Brune, and S. Gleyzes, A sensitive electrometer based on a Rydberg atom in a Schrödinger-cat state, Nature (London) **535**, 262 (2016).
[61] W. J. Munro, K. Nemoto, G. J. Milburn, and S. L. Braunstein, Weak-force detection with superposed coherent states, Phys. Rev. A **66**, 023819 (2002).
[62] N. Didier, A. Kamal, W. D. Oliver, A. Blais, and A. A. Clerk, Heisenberg-Limited Qubit Read-Out with Two-Mode Squeezed Light, Phys. Rev. Lett. **115**, 093604 (2015).
[63] S. Schreppler, N. Spethmann, N. Brahms, T. Botter, M. Barrios, and D. M. Stamper-Kurn, Optically measuring force near the standard quantum limit, Science **344**, 1486 (2014).
[64] D. Mason, J. Chen, M. Rossi, Y. Tsaturyan, and A. Schliesser, Continuous force and displacement measurement below the standard quantum limit, Nat. Phys. **15**, 745 (2019).
[65] W. Wang, Y. Wu, Y. Ma, W. Cai, L. Hu, X. Mu, Y. Xu, Z.-J. Chen, H. Wang, Y. P. Song, H. Yuan, C.-L. Zou, L.-M. Duan, and L. Sun, Heisenberg-limited single-mode quantum metrology in a superconducting circuit, Nat. Commun. **10**, 4382 (2019).
[66] M. Zwierz, C. A. Pérez-Delgado, and P. Kok, General Optimality of the Heisenberg Limit for Quantum Metrology, Phys. Rev. Lett. **105**, 180402 (2010).
[67] C. Gerry and P. L. Knight, *Introductory Quantum Optics* (Cambridge University, Cambridge, 2005).
[68] V. V. Dodonov and V. I. Man'ko, *Theory of Nonclassical States of Light* (Taylor & Francis, New York, 2003), and some references therein .
[69] A. Joshi and A.-S. F. Obada, Some statistical properties of the even and the odd negative binomial states, J. Phys. A: Math. Gen. **30**, 81 (1997).
[70] F. A. El-Orany, J. Peřina, and M. Sebawe Abdalla, Quantum properties of the parametric amplifier with and without pumping field fluctuations, Opt. Commun. **187**, 199 (2001).
[71] D. F. Walls and G. J. Milburn, *Quantum Optics* (Springer, Berlin, 2008).
[72] C. W. Helstrom, Quantum detection and estimation theory, J. Stat. Phys. **1**, 231 (1969).
[73] B. M. Escher, R. L. de Matos Filho, and L. Davidovich, General framework for estimating the ultimate precision limit in noisy quantum-enhanced metrology, Nat. Phys. **7**, 406 (2011); Quantum metrology for noisy systems, Braz. J. Phys. **41**, 229 (2011).
[74] R. A. Fisher, On the mathematical foundations of theoretical statistics, Philos. Trans. R. Soc. London Ser. A **222**, 309 (1922).
[75] R. A. Fisher, Theory of statistical estimation, Math. Proc. Camb. Philos. Soc. **22**, 700 (1925).
[76] H. Cramér, *Mathematical Methods of Statistics* (Princeton University Press, Princeton, 1999).
[77] C. R. Rao, *Linear Statistical Inference and its Applications* (Wiley, New York, 1973), Vol. 2.
[78] M. Woolley, G. Milburn, and C. M. Caves, Nonlinear quantum metrology using coupled nanomechanical resonators, New J. Phys. **10**, 125018 (2008).
[79] M. Napolitano and M. Mitchell, Nonlinear metrology with a quantum interface, New J. Phys. **12**, 093016 (2010).
[80] D. Tsarev, T. Ngo, R.-K. Lee, and A. Alodjants, Nonlinear quantum metrology with moving matter-wave solitons, New J. Phys. **21**, 083041 (2019).

[81] C. M. Caves, Quantum-mechanical noise in an interferometer, Phys. Rev. D **23**, 1693 (1981).

[82] L. Pezzé and A. Smerzi, Mach-Zehnder Interferometry at the Heisenberg Limit with Coherent and Squeezed-Vacuum Light, Phys. Rev. Lett. **100**, 073601 (2008).

[83] J. Sahota and N. Quesada, Quantum correlations in optical metrology: Heisenberg-limited phase estimation without mode entanglement, Phys. Rev. A **91**, 013808 (2015).

[84] L. G. Lutterbach and L. Davidovich, Method for Direct Measurement of the Wigner Function in Cavity QED and Ion Traps, Phys. Rev. Lett. **78**, 2547 (1997).